Journal of Applied Physics

RESEARCH ARTICLE | FEBRUARY 17 2026

# Halide vapor phase epitaxy of a thick *c*-plane α-$Ga_2O_3$ film on a high-quality α-$Cr_2O_3$/sapphire template

Yuichi Oshima ; Takayoshi Oshima ; Shiyu Xiao ; Kazuto Murakami; Katsuhiro Imai; Takahiro Tomita



*J. Appl. Phys.* 139, 075302 (2026)
https://doi.org/10.1063/5.0319104









AIP Publishing

Journal of Applied Physics ARTICLE pubs.aip.org/aip/jap

# Halide vapor phase epitaxy of a thick *c*-plane α-$Ga_2O_3$ film on a high-quality α-$Cr_2O_3$/sapphire template

Cite as: J. Appl. Phys. **139**, 075302 (2026); doi: 10.1063/5.0319104
Submitted: 22 December 2025 · Accepted: 28 January 2026 ·
Published Online: 17 February 2026



Yuichi Oshima,[1,a)] Takayoshi Oshima,[1] Shiyu Xiao,[2] Kazuto Murakami,[2] Katsuhiro Imai,[2] and Takahiro Tomita[2]

## AFFILIATIONS

[1]Research Center for Electronic and Optical Materials, National Institute for Materials Science, 1-1 Namiki, Tsukuba 305-0044, Japan
[2]NGK Insulators, Ltd, 2-56 Suda-cho, Mizuho, Nagoya 467-8530, Japan

[a)]**Author to whom correspondence should be addressed:** OSHIMA.Yuichi@nims.go.jp

## ABSTRACT

α-$Ga_2O_3$ is a promising ultra-wide-bandgap semiconductor for future power devices, and the use of α-$Cr_2O_3$ buffer layers represents an effective approach to improve the crystalline quality of heteroepitaxial α-$Ga_2O_3$ films owing to the small lattice mismatch between the two materials. In this study, *c*-plane α-$Ga_2O_3$ films were grown using halide vapor phase epitaxy (HVPE) on high-quality α-$Cr_2O_3$/sapphire templates, and the dependence of crystalline quality on the film thickness was systematically investigated. HVPE growth was performed under atmospheric pressure at 520 °C using GaCl and $O_2$ as the precursors and at a growth rate of 14 $\mu$m $h^{-1}$. The film thickness was varied from 0.24 to 21 $\mu$m by controlling the growth time. X-ray 2$\theta$–$\omega$ scan and pole figure measurements helped confirm that the α-$Ga_2O_3$ epilayers were phase-pure single-crystalline films. Thickness-dependent x-ray rocking curve measurements and reciprocal space mapping revealed that lattice relaxation began at a thickness of approximately 0.47 $\mu$m or less and virtually completed at thicknesses of 11 $\mu$m or greater. Cross-sectional scanning transmission electron microscopy results showed that dislocations were observed predominantly near the film surface and were absent at the α-$Ga_2O_3$/α-$Cr_2O_3$ interface. Etch-pit density measurements yielded a low dislocation density of $5.6 \times 10^7$ $cm^{-2}$ for the fully strained 0.24 $\mu$m-thick film. The almost fully relaxed 21 $\mu$m-thick film showed a higher dislocation density of $3.9 \times 10^8$ $cm^{-2}$. Nevertheless, this value was approximately one order of magnitude lower than that of an α-$Ga_2O_3$ film directly grown on a *c*-plane sapphire substrate under identical conditions.





## I. INTRODUCTION

Corundum-structured α-$Ga_2O_3$ is an ultra-wide-bandgap semiconductor exhibiting the highest bandgap energy among $Ga_2O_3$ polymorphs ($E_g = 5.3$ eV).[1] Owing to the large bandgap, a high critical electric field is expected, which is advantageous for power device applications. Moreover, α-$Ga_2O_3$ can form solid solutions without compositional limitations with other corundum-structured oxides, such as α-$Al_2O_3$, providing a high degree of freedom for band engineering.[2] Although it is difficult to impart *p*-type conduction to α-$Ga_2O_3$, isomorphic *p*-type oxides, such as α-$(Ir,Ga)_2O_3$, can be utilized to form hetero-*pn* junctions.[3–5] These characteristics make α-$Ga_2O_3$ a promising material for future high-performance power devices. In fact, several promising prototype devices have been reported, including Schottky barrier diodes (SBDs) with a very low on-resistance of 0.1 mΩ $cm^2$,[6] ampere-class SBDs with a breakdown voltage ($V_B$) of 1.7 kV,[7] and metal-oxide-semiconductor field-effect transistors with a $V_B$ of 2.3 kV.[8]

α-$Ga_2O_3$ can be grown using various epitaxial growth techniques, including mist chemical vapor deposition (mist CVD),[1,3] halide vapor phase epitaxy (HVPE),[9,10] molecular beam epitaxy,[11–13] and metal-organic vapor phase epitaxy.[14] To date, sapphire substrates have been predominantly used for growing

α-$Ga_2O_3$. This is because sapphire shares the same corundum crystal structure as α-$Ga_2O_3$ and, high-quality, large-area sapphire substrates are commercially available at a reasonable cost.

However, due to the large lattice mismatch between sapphire and α-$Ga_2O_3$ ($\Delta a/a = -4.5\%$ and $\Delta c/c = -3.3\%$), an α-$Ga_2O_3$ epilayer grown on sapphire substrates without any specific countermeasures exhibits an extremely high dislocation density. For example, regarding α-$Ga_2O_3$ grown on *c*-plane sapphire substrates, Kaneko *et al.* reported that the dislocation density of a film grown by mist CVD was approximately $7 \times 10^{10}$ $cm^{-2}$ in the vicinity of the interface (~100 nm).[15] In addition, Oshima *et al.* reported a dislocation density of approximately $3 \times 10^{10}$ $cm^{-2}$ in a 4-μm-thick HVPE-grown film.[16] Such a high dislocation density can lead to a deterioration in device performance. For example, carrier scattering by dislocations may reduce carrier mobility.[17] According to the theoretical calculations made by Takane *et al.*, carrier scattering at a carrier concentration of $1 \times 10^{16}$ $cm^{-3}$ should be negligible when the dislocation density is $1 \times 10^{8}$ $cm^{-2}$ or lower.[17]

Several techniques have been reported to reduce the dislocation density in α-$Ga_2O_3$ epilayers, such as epitaxial lateral overgrowth[16,18,19] and low-temperature high-growth-rate techniques.[20] By employing these approaches, dislocation densities below $1 \times 10^{8}$ $cm^{-2}$ can be achieved.[19,20] However, they require lithography-based mask formation and/or relatively thick film growth, posing challenges in terms of manufacturing cost.

In recent years, a corundum-structured α-$Cr_2O_3$ buffer layer has attracted considerable attention as a novel approach for reducing the dislocation density in α-$Ga_2O_3$ epilayers. This is because the lattice mismatch between α-$Cr_2O_3$ and α-$Ga_2O_3$ ($\Delta a/a = -0.45\%$ and $\Delta c/c = 1.23\%$) is significantly lower than that between sapphire and α-$Ga_2O_3$. Several studies have reported the epitaxial growth of α-$Ga_2O_3$ on a sapphire substrate using an α-$Cr_2O_3$ film as the buffer layer.[21–23]

Stepanov *et al.* grew α-$Ga_2O_3$ using HVPE on a *c*-plane sapphire substrate on which a 150-nm-thick *c*-plane α-$Cr_2O_3$ layer had been deposited by radio frequency magnetron sputtering. The full widths at half maximum (FWHMs) of the x-ray rocking curves (XRCs) for the 0006 (symmetric) and $10\bar{1}8$ (skew-symmetric) diffractions were both approximately 1400 arcsec. In contrast, for α-$Ga_2O_3$ grown directly on sapphire, the corresponding values were 60 and 2400 arcsec, respectively. From these XRC-FWHM values, the dislocation density was estimated to decrease from $2 \times 10^{10}$ to $5 \times 10^{9}$ $cm^{-2}$, owing to the introduction of the α-$Cr_2O_3$ buffer layer.[21]

However, this dislocation density is still high, which is likely attributable to the insufficient crystalline quality of the α-$Cr_2O_3$ buffer layer. The small lattice mismatch between α-$Ga_2O_3$ and α-$Cr_2O_3$ implies that α-$Ga_2O_3$ largely inherits its crystalline quality from the underlying α-$Cr_2O_3$ layer. Therefore, the α-$Cr_2O_3$ buffer layer must itself have a high crystalline quality to obtain high-quality α-$Ga_2O_3$ epilayers.

Recently, a template comprising a high-quality, approximately 100-μm-thick *c*-plane α-$Cr_2O_3$ layer formed on a *c*-plane sapphire substrate has been realized by a group at NGK Insulators, Ltd. Although the specific methods used to grow the α-$Cr_2O_3$ layer have not been disclosed, the FWHMs of the XRCs for the 0006 (symmetric) and $10\bar{1}4$ (skew-symmetric) diffractions were reported to be approximately 100 and 120 arcsec, respectively.[22]

Several studies have reported the growth of *c*-plane α-$Ga_2O_3$ on such high-quality α-$Cr_2O_3$ templates.[22,23] Yamada *et al.* deposited an approximately 0.7-μm-thick α-$Ga_2O_3$ layer using mist CVD; the dislocation density, estimated from the XRC-FWHM values, was $4 \times 10^{7}$ $cm^{-2}$, which is approximately three orders of magnitude lower than that of α-$Ga_2O_3$ grown directly on sapphire substrates.[22] Takeda *et al.* reported the growth of a phase-pure α-$Ga_2O_3$ film using HVPE, for which the XRC-FWHMs of the 0006 and $10\bar{1}4$ diffractions were 250 and 290 arcsec, respectively (the film thickness was not specified).[23] Based on these XRC-FWHM values, the dislocation density of this film was considered to be of the order of $10^{8}$ $cm^{-2}$.

Clearly, the use of high-quality α-$Cr_2O_3$ templates appears to be effective in improving the crystalline quality of α-$Ga_2O_3$. However, this effectiveness has, thus, far been demonstrated primarily for thin films with thicknesses of less than approximately 1 μm. From the viewpoint of applications to α-$Ga_2O_3$-based vertical power devices, it is essential to verify the effectiveness of such templates for thick films suitable for use as drift layers. Therefore, in this study, *c*-plane α-$Ga_2O_3$ layers with thicknesses of up to 21 μm were grown at a high-growth rate using HVPE on high-quality *c*-plane α-$Cr_2O_3$ templates, and the thickness dependence of their crystalline quality was systematically investigated.

## II. EXPERIMENTAL

α-$Ga_2O_3$ was grown using a laboratory-made atmospheric-pressure HVPE reactor at a temperature of 520 °C. $O_2$ (>99.999 95% purity) and GaCl were used as precursors. GaCl was synthesized *in situ* upstream in the reactor by the reaction between Ga metal (>99.999 99% purity) and HCl gas (>99.999% purity) at a temperature of 570 °C. The partial pressures of $O_2$ and GaCl were set to 1.25 kPa and 125 Pa, respectively. In addition to these precursors, HCl gas was directly supplied to the growth zone at a partial pressure of 188 Pa to suppress parasitic reactions.[10] $N_2$ (dew point < −110 °C) was used as the carrier gas. Under these growth conditions, the growth rate was approximately 14 μm $h^{-1}$. By varying the growth time, α-$Ga_2O_3$ layers were grown with thicknesses (*t*) ranging from 0.24 to 21 μm.

We used high-quality *c*-plane α-$Cr_2O_3$/sapphire templates (manufactured by NGK Insulators, Ltd) for the HVPE growth. The thickness of the α-$Cr_2O_3$ layer was approximately 100 μm. The XRC-FWHMs for the 0006 and $10\bar{1}4$ diffractions of the α-$Cr_2O_3$ layer were typically less than approximately 100 and 200 arcsec, respectively. The templates were cleaned using hydrofluoric acid and a sulfuric acid–hydrogen peroxide mixture prior to the HVPE growth.

The phase purity and crystallographic orientation of the grown epilayers were examined by x-ray 2θ–ω scan and pole figure measurements, respectively. The crystalline quality was evaluated based on the XRC-FWHMs for the 0006 (symmetric) and $10\bar{1}4$ (skew-symmetric) diffractions, denoted by $\beta(0006)$ and $\beta(10\bar{1}4)$, respectively. The parameter $\beta(0006) \equiv \beta_{tilt}$ is referred to as the tilt angle and represents the tilt spread of the *c*-plane. The twist angle $\beta_{twist}$, which characterizes the twist spread about the *c* axis, was calculated using the following relationship:[24,25]

$$\beta(10\bar{1}4)^2 = (\beta_{tilt}\cos\chi)^2 + (\beta_{twist}\sin\chi)^2, \quad (1)$$

where χ is the inclination angle of the diffracting plane $(10\bar{1}4)$.

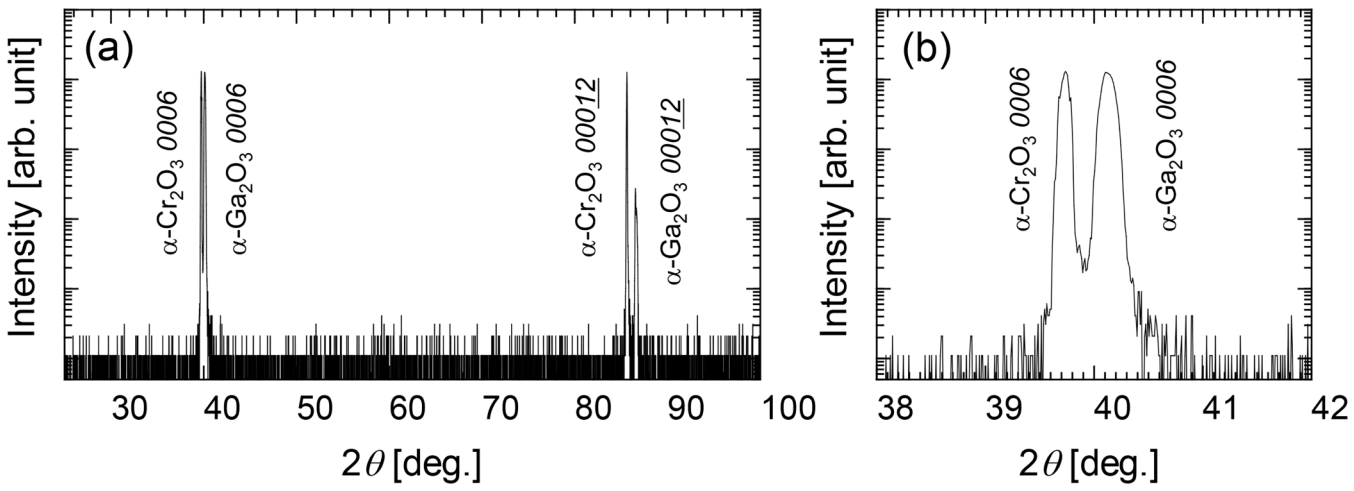


**FIG. 1.** (a) X-ray $2\theta$–$\omega$ scan profile of an α-$Ga_2O_3$ ($t = 2.4$ μm)/α-$Cr_2O_3$/sapphire epiwafer. (b) Enlarged view of (a).

Both the templates and grown epiwafers exhibited convex wafer bowing, with relatively large curvatures ranging from −0.3 to −1.8 $m^{-1}$, as shown in Fig. S1 in the supplementary material. To minimize the influence of wafer curvature on the XRC-FWHM values, an optimized optical configuration was employed, and curvature-induced broadening was corrected based on the measured curvature of each sample. The values of $\beta(hkml)$ used in this study correspond to those obtained after curvature correction. Detailed descriptions of the optical setup and the curvature correction procedure are provided in Appendix A.

The strain state of the α-$Ga_2O_3$ films was evaluated by x-ray reciprocal space mapping (RSM) of the $\bar{2}02\underline{10}$ diffractions. For the $\bar{2}02\underline{10}$ diffractions of α-$Ga_2O_3$, the x-ray incidence angle to the epilayer surface was 74.399°, which corresponds to the sum of the Bragg angle (42.492°) and the angle between the (0001) and ($\bar{1}$015) planes (31.907°).

The dislocation behavior was investigated by cross-sectional scanning transmission electron microscopy (STEM) observations from the $m$ axis direction. Dislocation types were identified using the $g \cdot b = 0$ criterion under two-beam dark-field conditions with $g = 0006$ and $11\bar{2}0$. The dislocation density was estimated either from the XRC-FWHM values[26] or by measuring the etch-pit density (EPD) using HCl gas etching.[27] See Appendix B for the specific procedure for EPD estimation.

## III. RESULTS AND DISCUSSION

Figure 1(a) shows the x-ray $2\theta$–$\omega$ scan profile of a 2.4-$\mu$m-thick α-$Ga_2O_3$ epilayer measured in the out-of-plane configuration; Fig. 1(b) presents an enlarged view of the profile. Only diffraction peaks originating from the (0001) planes of α-$Ga_2O_3$ and α-$Cr_2O_3$ can be observed. It should be noted that the theoretical transmittance of a 100-$\mu$m-thick α-$Cr_2O_3$ film (linear absorption coefficient of $8.989 \times 10^2$ $cm^{-1}$ for Cu K$\alpha_1$ radiation)[28] is only about 3.3 ppm, even when x rays are incident at the Bragg angle of sapphire $00\underline{12}$ diffraction ($\theta_B = 45.36°$). Therefore, the intensity of x rays that reach the sapphire substrate is diffracted, and subsequently transmits through the α-$Cr_2O_3$ film again to be detected should be virtually zero. This explains why no diffraction peaks from the sapphire substrate are observed in the 2θ–ω scan profile in Fig. 1. Figures 2(a) and 2(b) show the XRD pole figures for the $10\bar{1}4$ diffractions of α-$Ga_2O_3$ and α-$Cr_2O_3$, respectively. In both cases, diffraction peaks were observed only at the positions expected for single crystals with a corundum structure. These results confirm that the epilayer grown was a phase-pure, single-crystalline α-$Ga_2O_3$ film.

Figures 3(a) and 3(b) show the thickness dependences of $\beta_{tilt}$ and $\beta_{twist}$, respectively. The $\beta_{tilt}$ values of the α-$Ga_2O_3$ epilayers were close to those of the underlying α-$Cr_2O_3$ layer and did not significantly increase with increasing film thickness. In contrast, $\beta_{twist}$ remained comparable to that of the α-$Cr_2O_3$ layer up to a thickness of $t = 2.4$ $\mu$m but began to increase markedly at approximately $t \approx 5.9$ $\mu$m, followed by a substantial increase at larger thicknesses. The slight reduction in $\beta_{twist}$ observed at $t = 21$ $\mu$m compared with that at $t = 11$ $\mu$m may be attributed to dislocation annihilation occurring during thick-film growth.[20,29] It should be noted that a pronounced increase in $\beta_{twist}$ of α-$Cr_2O_3$ was observed for the sample with $t = 21$ $\mu$m. Although the origin of this behavior is not clear at present, this sample exhibited a much larger curvature than the other samples, as shown in Fig. S1 in the supplementary material. Therefore, we speculate that a large stress was applied to this sample, which may have resulted in the generation of dislocations in the α-$Cr_2O_3$ layer. However, this possibility has not been verified at this stage, and further investigation is required.

Figures 4(a)–4(f) show the RSM measurement results. At $t = 0.24$ $\mu$m, the in-plane lattice constant of α-$Ga_2O_3$ coincides with that of α-$Cr_2O_3$, indicating that the α-$Ga_2O_3$ epilayer was fully strained. At $t = 0.47$ $\mu$m, the α-$Ga_2O_3$ peak remains located at the fully strained position; however, its tail appears to extend toward

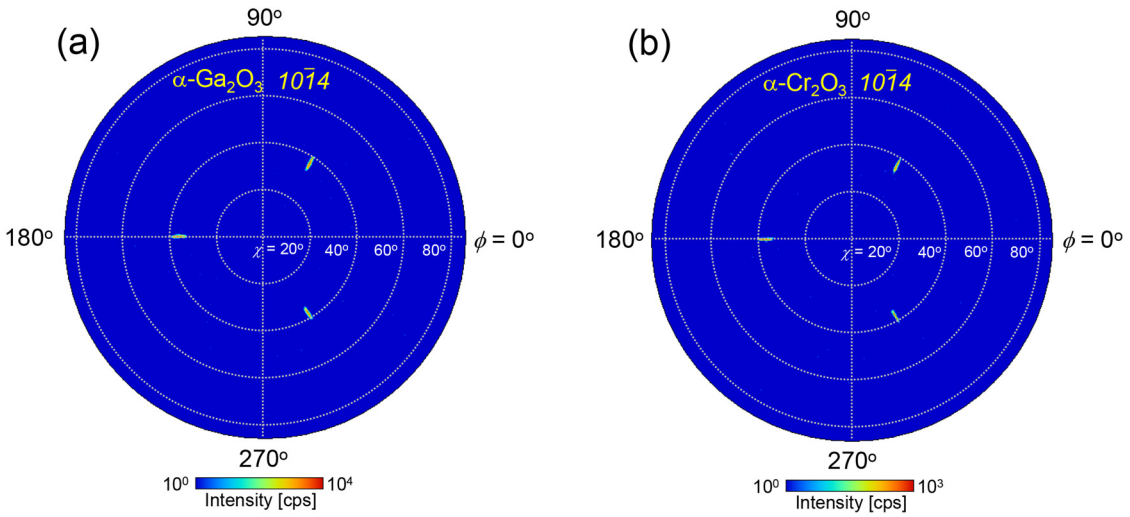


**FIG. 2.** X-ray pole figures of the α-$Ga_2O_3$ ($t = 2.4\ \mu$m)/α-$Cr_2O_3$/sapphire epiwafer measuring the 10$\bar{1}$4 diffractions of (a) α-$Ga_2O_3$ and (b) α-$Cr_2O_3$.

the fully relaxed position, suggesting the onset of lattice relaxation. At $t = 2.4$ and $5.9\ \mu$m, the α-$Ga_2O_3$ peak is still centered at the fully strained position, while the changes in the peak tail become more pronounced. For $t \geq 11\ \mu$m, the α-$Ga_2O_3$ peak is almost completely relaxed. The pronounced relaxation observed for $t \geq 11\ \mu$m is consistent with the thickness dependence of $\beta_{twist}$.

Based on our RSM measurements, lattice relaxation was observed when $t \geq 0.47\ \mu$m. Therefore, the critical thickness is likely to lie between 0.24 and $0.47\ \mu$m. The theoretical critical thickness of *c*-plane α-$Ga_2O_3$ grown on bulk α-$Cr_2O_3$ is estimated to be $0.36\ \mu$m based on the model proposed by People and Bean.[30] This value is in good agreement with the experimental results. In this calculation, lattice relaxation was assumed to occur via the introduction of edge dislocations with the Burgers vectors being equal to the *a* axis lattice constant. Table I presents the parameters used in the calculation.

Figure 5(a) shows a cross-sectional bright-field STEM image of the sample with $t = 5.9\ \mu$m, which is considered to be partially relaxed. No dislocations were observed at the α-$Ga_2O_3$/α-$Cr_2O_3$ interface, whereas dislocations were clearly observed near the surface of the α-$Ga_2O_3$ layer. Typically, lattice relaxation in a lattice-mismatched heteroepitaxial system proceeds via the



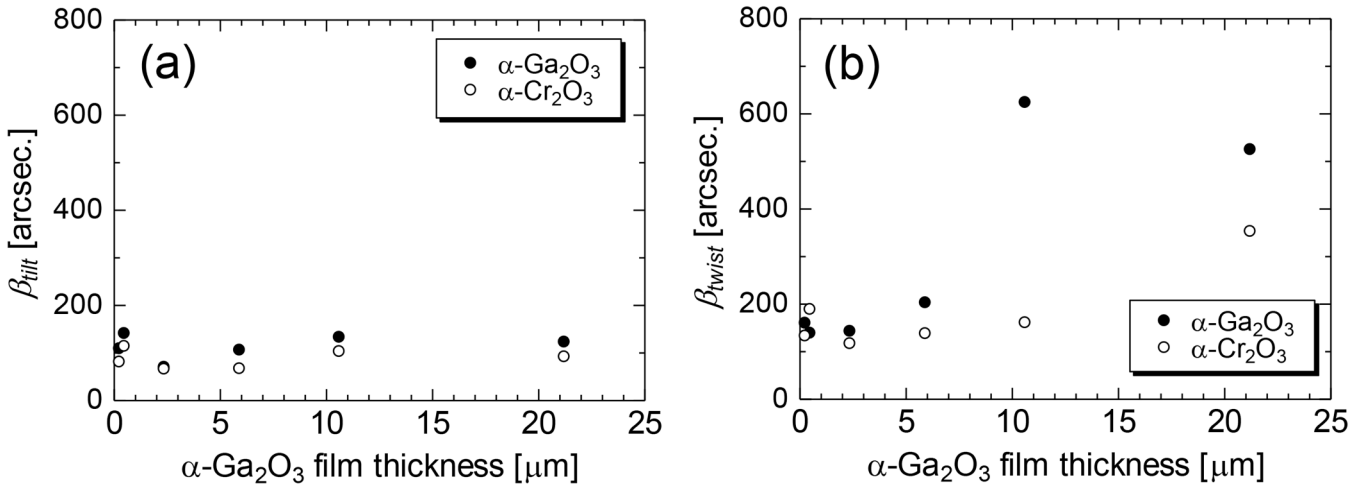


**FIG. 3.** (a) Tilt and (b) twist angles of the α-$Ga_2O_3$ film and α-$Cr_2O_3$ template layer estimated based on the XRC measurements as a function of the α-$Ga_2O_3$ film thickness.

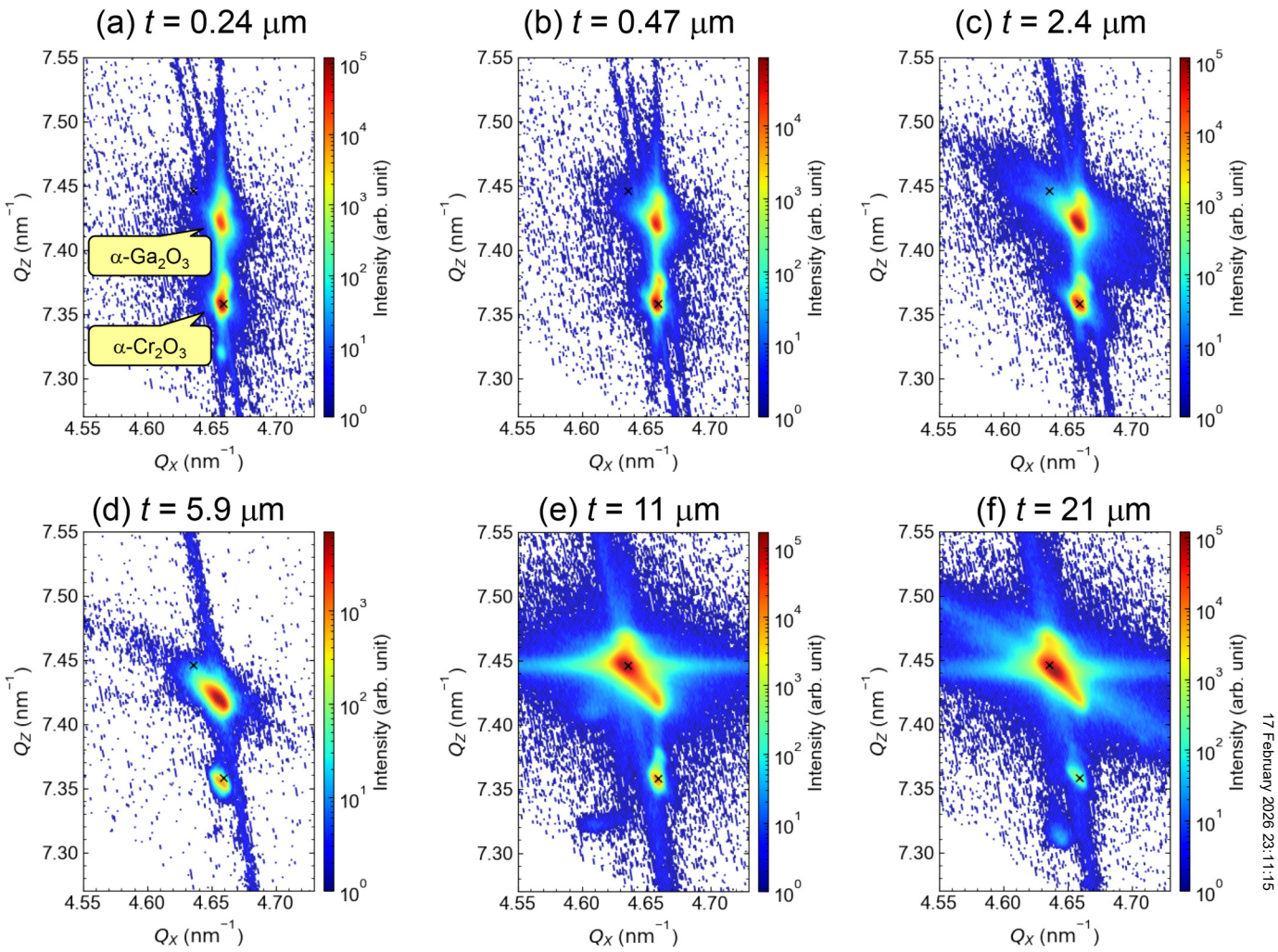


**FIG. 4.** Reciprocal space mapping (RSM) of $\alpha$-$Ga_2O_3$/$\alpha$-$Cr_2O_3$/sapphire epiwafers with various $\alpha$-$Ga_2O_3$ film thicknesses. Fully relaxed positions for $\alpha$-$Ga_2O_3$ and $\alpha$-$Cr_2O_3$ are indicated by × marks.

nucleation of dislocation half-loops on the surface, which expand by gliding toward the interface and eventually form threading dislocations and misfit dislocations therein. In Fig. 5(a), the fact that dislocations are observed only near the surface and did not reach the interface appears to be consistent with the RSM results, indicating that this sample was at a relatively early stage of lattice relaxation. Figures 5(b)–5(d) show two-beam dark-field TEM images of the dislocations observed in Fig. 5(a). Since the contrast of most of the dislocations disappeared under the $g = 0006$ condition, the majority of dislocations were inferred to be edge-type. This observation is consistent with the results shown in Fig. 3, where the increase in crystallographic orientation fluctuations with increasing film thickness is dominated by the twist component. It should be noted that the periodic fringe patterns and dark line-like contrasts observed in Figs. 5(c) and 5(d) are attributed to equal-thickness fringes and bend contours, respectively, and are not associated with crystallographic defects.

Figure 6 shows the thickness dependence of the dislocation density estimated either from the XRC measurements or from the

**TABLE I.** Parameters used in calculating the critical thickness of c-plane $\alpha$-$Ga_2O_3$ grown on bulk $\alpha$-$Cr_2O_3$.

| Parameter | | Value | Source |
|---|---|---|---|
| *a* axis length | $\alpha$-$Ga_2O_3$ | 0.498 26 nm | PDF card No: 01-074-1610 |
| | $\alpha$-$Cr_2O_3$ | 0.496 00 nm | PDF card No. 01-070-3765 |
| Poisson's ratio | | 0.729 | First-principles calculation[31] |

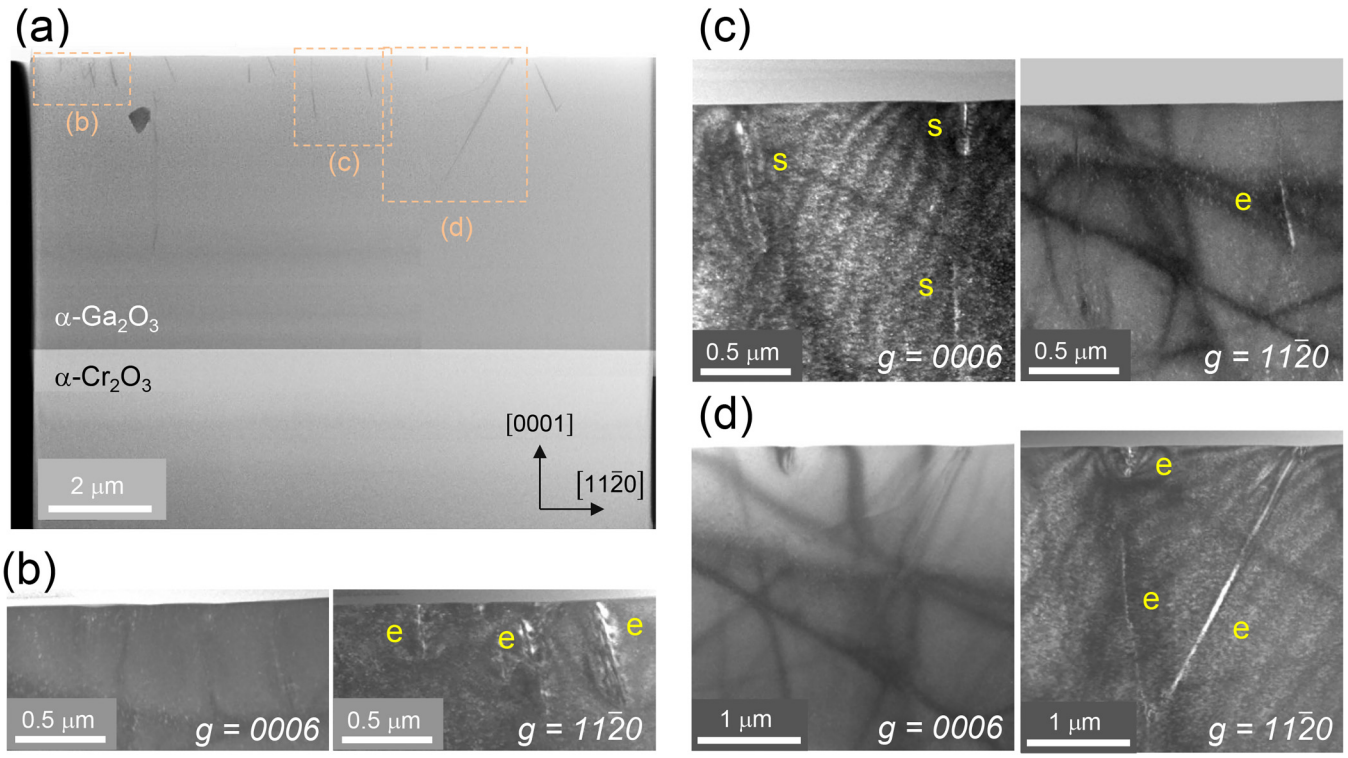


**FIG. 5.** (a) Bright-field cross-sectional STEM image of the α-$Ga_2O_3$ ($t = 5.9\ \mu m$)/α-$Cr_2O_3$/sapphire epiwafer. (b)–(d) Dark-field TEM images of dislocations observed under two-beam conditions. Dislocations considered to have edge and screw components are labeled *e* and *s*, respectively.

EPD measurements. For comparison, the figure also shows the EPD of an α-$Ga_2O_3$ film with $t = 21\ \mu m$ grown directly on a *c*-plane sapphire substrate under the same HVPE conditions. The edge and screw components of the dislocation density, $D_e$ and $D_s$, estimated from the XRC results were calculated using Eqs. (2) and (3), respectively,

$$D_e = \frac{\beta_{twist}^2}{(2\pi \ln 2) b_e^2}, \tag{2}$$

$$D_s = \frac{\beta_{tilt}^2}{(2\pi \ln 2) b_s^2}, \tag{3}$$

where, $b_e$ and $b_s$ denote the Burgers vectors of the edge and screw dislocations, respectively, for which $b_e = 0.498\ 25$ nm (the *a* axis lattice constant) and $b_s = 1.343\ 31$ nm (the *c* axis lattice constant) were used.[26] The dislocation densities estimated from the XRC measurements shown in Fig. 6 represent the sum of the edge and screw components.

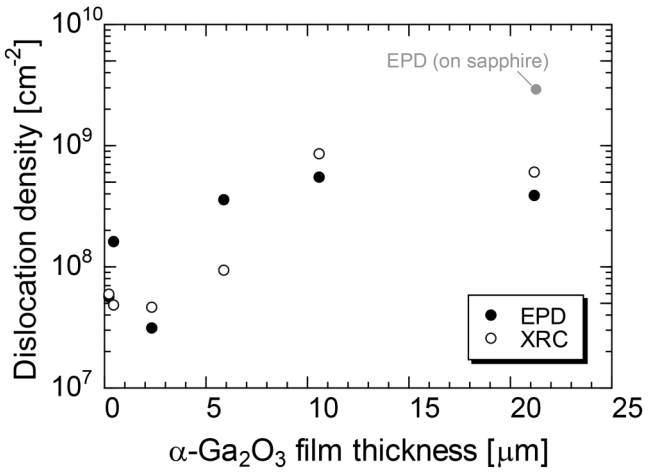


**FIG. 6.** Dislocation density of α-$Ga_2O_3$ epilayers estimated based on XRC measurements or by etch-pit counting as a function of the film thickness.

The dislocation density determined using the EPD method increased with increasing film thickness, similar to the trend observed in the XRC-based results. However, in the thickness range of $t \leq 5.9\ \mu m$, the EPD did not fully coincide with the lattice relaxation behavior inferred from the XRC and RSM results. This discrepancy is likely attributable to the nonuniform distribution of etch pits, as revealed by the Nomarski microscopy image in Fig. S3 in the supplementary material, which presumably reflects spatial inhomogeneity in the crystalline quality of the α-$Cr_2O_3$ template. It should be noted that the dislocation density distribution in the α-$Cr_2O_3$ layer was not investigated in this study, because the dislocation density was too low to evaluate the distribution by TEM

observations. To clarify the dislocation distribution in the α-$Cr_2O_3$ layer in the future, it will be necessary to establish an etch-pit-based method. Because the measurement area of the EPD (approximately $5 \times 13$–$10 \times 26\,\mu m^2$) was significantly lower than that probed by the XRC, the EPD was more susceptible to local variations in the dislocation density. Regardless of the estimation method, the dislocation density increased markedly for film thicknesses exceeding 5.9 μm. Nevertheless, even at large thicknesses, the dislocation density remained approximately one order of magnitude lower than that of an α-$Ga_2O_3$ film grown directly on a sapphire substrate.

## IV. CONCLUSIONS

α-$Ga_2O_3$ epilayers with thicknesses of up to 21 μm were grown using HVPE on high-quality *c*-plane α-$Cr_2O_3$/sapphire templates, and the thickness dependence of their crystalline properties was systematically investigated. Although the HVPE growth was performed at a high-growth rate of $14\,\mu m\,h^{-1}$, phase-pure, single-crystalline α-$Ga_2O_3$ films were successfully obtained, as confirmed by x-ray 2θ–ω scans and pole figure measurements. The tilt and twist spreads of the α-$Ga_2O_3$ epilayers were evaluated based on XRC measurements of the 0006 and $10\bar{1}4$ diffractions. The tilt spread did not significantly increase with increasing film thickness. In contrast, the twist spread began to increase at approximately $t = 5.9\,\mu m$ and showed a pronounced increase for $t \geq 11\,\mu m$. This relaxation behavior was also consistently observed in the RSM results. The dislocation density estimated by etch-pit counting was approximately $5.6 \times 10^7\,cm^{-2}$ for the thinnest, fully strained sample ($t = 0.24\,\mu m$), which was comparable to that of the template layer. In contrast, the dislocation density increased to $3.9 \times 10^8\,cm^{-2}$ for the virtually fully relaxed sample with $t = 21\,\mu m$. Nevertheless, this value remained substantially lower than that of the α-$Ga_2O_3$ film grown directly on a sapphire substrate under the same conditions ($3 \times 10^9\,cm^{-2}$). To suppress carrier scattering by dislocations, further reduction in the dislocation density would be required. From this perspective, continued development of template layers with even smaller lattice mismatches is highly desirable.

## SUPPLEMENTARY MATERIAL

See the supplementary material for the epiwafer curvature, measured XRC-FWHMs before and after the curvature correction, and optical microscopy image exhibiting the inhomogeneous etch-pit distribution.

## AUTHOR DECLARATIONS

### Conflict of Interest

The authors have no conflicts to disclose.

### Author Contributions

**Yuichi Oshima:** Conceptualization (lead); Data curation (lead); Formal analysis (lead); Investigation (lead); Methodology (lead); Resources (lead); Visualization (lead); Writing – original draft (lead); Writing – review & editing (equal). **Takayoshi Oshima:** Conceptualization (supporting); Data curation (supporting); Formal analysis (supporting); Investigation (supporting); Methodology (supporting); Visualization (supporting); Writing – review & editing (equal). **Shiyu Xiao:** Conceptualization (supporting); Data curation (supporting); Formal analysis (supporting); Investigation (supporting); Methodology (supporting); Resources (equal); Visualization (supporting); Writing – review & editing (equal). **Kazuto Murakami:** Conceptualization (supporting); Data curation (supporting); Formal analysis (supporting); Investigation (supporting); Methodology (supporting); Resources (equal); Visualization (supporting); Writing – review & editing (equal). **Katsuhiro Imai:** Conceptualization (supporting); Data curation (supporting); Formal analysis (supporting); Investigation (supporting); Methodology (supporting); Resources (equal); Visualization (supporting); Writing – review & editing (equal). **Takahiro Tomita:** Conceptualization (supporting); Data curation (supporting); Formal analysis (supporting); Investigation (supporting); Methodology (supporting); Resources (equal); Visualization (supporting); Writing – review & editing (equal).

## DATA AVAILABILITY

The data that support the findings of this study are available within the article and its supplementary material.

## APPENDIX A: OPTICAL SETUP AND CURVATURE CORRECTION PROCEDURE FOR XRC MEASUREMENTS

The α-$Cr_2O_3$/sapphire templates used in this study exhibited a curvature of approximately $-0.3\,m^{-1}$ prior to the epitaxial growth of α-$Ga_2O_3$, most likely due to the thermal stress arising from the difference in thermal expansion coefficients. Upon epitaxial growth of α-$Ga_2O_3$, the curvature further increased with increasing film thickness, reaching a value of $-1.8\,m^{-1}$ for the sample with a thickness of 21 μm. For samples with such a large curvature, the contribution of wafer bowing to the broadening of the XRC-FWHM may no longer be negligible.

To minimize the influence of epiwafer bowing on the XRC-FWHM values, the thickness of the incident x-ray beam was reduced to $h = 0.096$ mm using an incident slit. Under this condition, the length of the beam footprint in the direction perpendicular to the rocking axis during the 0006 XRC measurement, FP(0006), was 0.28 mm, as given by $FP(0006) = h/\sin\theta_{0006}$.

A parallel-plate collimator (PPC) with a receiving angle of 0.09° was placed in front of the x-ray detector. A slit was further installed to allow the x-ray beam to pass through only one of the multiple gaps of the PPC, with a gap width of 0.130 mm. Consequently, the effective beam footprint length on the sample in the direction perpendicular to the rocking axis during the $10\bar{1}4$ XRC measurement, FP($10\bar{1}4$), was limited to 0.45 mm, which can be expressed as $FP(10\bar{1}4) = \text{gap}/\sin\theta_{10\bar{1}4}$.

The peak broadening arising solely from wafer bowing, $\beta_r(hkml)$, can be expressed as $\beta_r(hkml) = FP(hkml)/R(hkml)$, where $R(hkml)$ is the radius of curvature for the $(hkml)$ plane.[24,25] The curvature radius $R(hkml)$ was determined from the peak shifts of the 0006 and $10\bar{1}4$ XRCs measured while translating the sample along the *x* axis.[32] Figure S1 in the supplementary material shows the relationship between the measured curvature, $R(hkml)^{-1}$, and the film thickness. Finally, the contribution of wafer bowing was removed using the following relationship to extract the intrinsic

XRC--FWHM, $\beta(hkml)$:[24,25]

$$\beta(hkml)^2 = \beta_m(hkml)^2 - \beta_r(hkml)^2, \quad \text{(A1)}$$

where $\beta_m(hkml)$ is the experimentally measured XRC-FWHM for the 0006 or $10\bar{1}4$ diffractions. Figures S2(a) and S2(b) in the supplementary material show the thickness dependences of $\beta_m(hkml)$; Figs. S2(c) and S2(d) in the supplementary material present the corresponding thickness dependences of the curvature-corrected values $\beta(hkml)$.

## APPENDIX B: PROCEDURE FOR EPD ESTIMATION

As shown in Fig. S3 in the supplementary material, the EPD of the α-$Ga_2O_3$ epilayer was not necessarily uniform. EPD values were particularly high in the vicinity of regions corresponding to macroscopic defects in the α-$Cr_2O_3$ layer, which were originally present at a density of approximately $10^3\ cm^{-2}$ and are indicated by the yellow circle in Fig. S3 in the supplementary material. Therefore, EPD in this study was estimated in regions located as far as possible from such macroscopic defects. In these regions, SEM observations were carried out at four randomly selected locations, and the average EPD was calculated. The observation magnification was chosen according to the dislocation density, such that the number of etch pits in each field of view was approximately more than ~100; magnifications of 5k× (field of view: $10 \times 26\,\mu m^2$) and 10k× (field of view: $5 \times 13\,\mu m^2$) were used as appropriate.

## REFERENCES


[1]D. Shinohara and S. Fujita, Jpn. J. Appl. Phys. **47**, 7311 (2008).
[2]H. Ito, K. Kaneko, and S. Fujita, Jpn. J. Appl. Phys. **51**, 100207 (2012).
[3]K. Kaneko, S. Fujita, and T. Hitora, Jpn. J. Appl. Phys. **57**, 117103 (2018).
[4]S. Kan, S. Takemoto, K. Kaneko, I. Takahashi, M. Sugimoto, T. Shinohe, and S. Fujita, Appl. Phys. Lett. **113**, 212104 (2018).
[5]K. Kaneko, Y. Masuda, S. Kan, I. Takahashi, Y. Kato, T. Shinohe, and S. Fujita, Appl. Phys. Lett. **118**, 102104 (2021).
[6]M. Oda, R. Tokuda, H. Kambara, T. Tanikawa, T. Sasaki, and T. Hitora, Appl. Phys. Express **9**, 021101 (2016).
[7]T. Shinohe, in 2024 *IEEE International Meeting for Future Electron Devices, Kansai* (IEEE, 2024), pp. 1–4.
[8]Y. J. Jeong, J. H. Park, M. J. Yeom, I. Kang, J. Y. Yang, H. Y. Kim, D. W. Jeon, and G. Yoo, Appl. Phys. Express **15**, 074001 (2022).
[9]Y. Oshima, E. G. Víllora, and K. Shimamura, Appl. Phys. Express **8**, 055501 (2015).
[10]Y. Oshima, K. Kawara, T. Oshima, M. Okigawa, and T. Shinohe, Semicond. Sci. Technol. **35**, 055022 (2020).
[11]Z. Cheng, M. Hanke, P. Vogt, O. Bierwagen, and A. Trampert, Appl. Phys. Lett. **111**, 162104 (2017).
[12]R. Jinno, C. S. Chang, T. Onuma, Y. Cho, S.-T. Ho, D. Rowe, M. C. Cao, K. Lee, V. Protasenko, D. G. Schlom, D. A. Muller, H. G. Xing, and D. Jena, Sci. Adv. **7**, eabd5891 (2021).
[13]J. Steele, J. Chen, T. Burrell, N. A. Pieczulewski, D. Bhattacharya, K. Smith, K. Gann, M. O. Thompson, H. G. Xing, D. Jena, D. A. Muller, M. D. Williams, M. K. I. Senevirathna, and D. G. Schlom, APL Mater. **13**, 101117 (2025).
[14]A. F. M. A. U. Bhuiyan, Z. Feng, H.-L. Huang, L. Meng, J. Hwang, and H. Zhao, APL Mater. **9**, 101109 (2021).
[15]K. Kaneko, H. Kawanowa, H. Ito, and S. Fujita, Jpn. J. Appl. Phys. **51**, 020201 (2012).
[16]Y. Oshima, K. Kawara, T. Shinohe, T. Hitora, M. Kasu, and S. Fujita, APL Mater. **7**, 022503 (2019).
[17]H. Takane, H. Izumi, H. Hojo, T. Wakamatsu, K. Tanaka, and K. Kaneko, J. Mater. Res. **38**, 2645 (2023).
[18]Y. Oshima, K. Kawara, T. Oshima, M. Okigawa, and T. Shinohe, Jpn. J. Appl. Phys. **59**, 025512 (2020).
[19]Y. Oshima and T. Shinohe, Appl. Phys. Lett. **126**, 202104 (2025).
[20]Y. Oshima, H. Ando, and T. Shinohe, Appl. Phys. Express **16**, 065501 (2023).
[21]S. I. Stepanov, V. I. Nikolaev, A. V. Almaev, A. I. Pechnikov, M. P. Scheglov, A. V. Chikiryaka, B. O. Kushnarev, and A. Y. Polyakov, Mater. Phys. Mech. **47**, 577 (2021).
[22]K. Yamada, R. Iida, S. Xiao, K. Murakami, T. Onuma, T. Honda, M. Watanabe, and T. Yamaguchi, "Mist CVD growth and characterization of α-$Ga_2O_3$ films on α-$Cr_2O_3$ templates," in *72nd JSAP Spring Meeting, Noda, Japan* (MDPI, 2025), p. 16p-Y1311-7.
[23]K. Takeda, Y. Morishita, S. Xiao, K. Murakami, M. Watanabe, T. Tomita, and R. Miyagawa, "Epitaxial growth of $Ga_2O_3$ on $Cr_2O_3$ template by HVPE," in *44th Electronic Materials Symposium (EMS-44), Nara, Japan* (EMS, 2025), p. Fr1-12.
[24]J. Q. Liu, J. F. Wang, Y. X. Qiu, X. Guo, K. Huang, Y. M. Zhang, X. J. Hu, Y. Xu, K. Xu, X. H. Huang, and H. Yang, Semicond. Sci. Technol. **24**, 125007 (2009).
[25]M. A. Moram and M. E. Vickers, Rep. Prog. Phys. **72**, 036502 (2009).
[26]T. C. Ma, X. H. Chen, Y. Kuang, L. Li, J. Li, F. Kremer, F.-F. Ren, S. L. Gu, R. Zhang, Y. D. Zheng, H. H. Tan, C. Jagadish, and J. D. Ye, Appl. Phys. Lett. **115**, 182101 (2019).
[27]Y. Oshima, S. Yagyu, and T. Shinohe, J. Cryst. Growth **576**, 126387 (2021).
[28]M. J. Berger, J. H. Hubbell, S. M. Seltzer, J. Chang, J. S. Coursey, R. Sukumar, D. S. Zucker, and K. Olsen, see https://www.nist.gov/pml/xcom-photon-cross-sections-database for "XCOM: Photon Cross Sections Database version 1.5" (2010).
[29]K. Fujito, S. Kubo, H. Nagaoka, T. Mochizuki, H. Namita, and S. Nagao, J. Cryst. Growth **311**, 3011 (2009).
[30]R. People and J. C. Bean, Appl. Phys. Lett. **47**, 322 (1985).
[31]T. Kawamura and T. Akiyama, Jpn. J. Appl. Phys. **61**, 021005 (2022).
[32]See https://rigaku.com/products/x-ray-diffraction-and-scattering/xrd/application-notes/b-xrd2031-curvature-single-crystal-substrate?setLang=english for "Rigaku application note B-XRD2031."